UDK 620.193.472/.479:621.311.2
Original scientific article/Izvirni znanstveni članek

ISSN 1580-2949
MTAEC9, 57(4)317(2023)

THERMAL-POWER-PLANT CONDENSER-TUBE CORROSION ANALYSIS

ANALIZA KOROZIJE NA KONDENZACIJSKI CEVI V TERMOELEKTRARNI

Jakov Batelić[1], Vedrana Špada[2], Marko Kršulja[3*], Sanja Martinez[4]

[1]HEP Production 52234 Plomin luka, Plomin luka 50, Sector for Thermal Power Plants, Plomin Power Plant Operation, Croatia
[2]Istrian Polytechnic, METRIS Materials Research Centre of the Region of Istria, Zagrebačka 30, 52100 Pula, Croatia
[3]University Juraj Dobrila of Pula, Faculty of Engineering, Zagrebačka 30, 52100 Pula, Croatia
[4]University of Zagreb, Faculty of Chemical Engineering and Technology, Department of Electrochemistry, Marulićev trg 19, 10 000 Zagreb, Croatia

Prejem rokopisa – received: 2023-01-14; sprejem za objavo – accepted for publication: 2023-05-15

doi:10.17222/mit.2023.747

The thermal-power-plant condenser tubes, conducting cooling seawater, experienced frequent leakages, prompting the hereby presented failure analysis. Visual inspection of the corroded/ruptured tube segments revealed that localized corrosion may be linked to seawater sediments and thick layers of corrosion products at the tube water side. Sediments were found along the tube bottom and thick corrosion products were found adjacent to the point of contact between the baffle plates and the exterior tube walls. Underdeposit corrosion, accelerated due to sulphate-reducing bacteria, was diagnosed based on the excess sulphur found at the pit bottom using EDX, the FT-IR spectrum indicating the presence of biofilm and SEM determining the featuring corrosion products based on the biofilm. It was proposed that the corrosion initiating deposits were linked to the condenser shutdown and startup periods. Results showed that pitting corrosion occurred under the influence of biofilm microorganisms tolerant to copper. The main goal of this research was achieved by defining a systematic procedure for avoiding a shutdown of the thermal power plant.

Keywords: corrosion, pitting, thermal power plant, condenser

Kondenzacijske cevi analiziranega primera, ki se nahajajo v termoelektrarni Plomin, Hrvaška prenašajo hladilno morsko vodo. Pri tem pogosto pride zaradi korozije do zaznavanja nenadnega puščanja cevi in potrebno je takojšnje ukrepanje oziroma odprava netesnosti. V pričujočem članku avtorji opisujejo analizo poškodb v enem od takšnih primerov. Vizualni pregled segmentov korodirane in poškodovane cevi je pokazal, da je lokalna korozija morda povezana z usedlinami iz morske vode in debelimi plastmi korozijskih produktov na vodni strani cevi. Usedline so avtorji našli vzdolžno na dnu cevi in debele plasti korozijskih produktov so se nahajale tudi v bližini stika med odbojnimi ploščami in zunanjimi stenami cevi. Korozija pod usedlino je bila pospešena zaradi delovanja sulfatnih redukcijskih bakterij, kar so avtorji potrdili s prisotnostjo prebitne vsebnosti žvepla na dnu korozijske jamice. Karakterizacijo mest na katerih je prišlo do korozijskih poškodb so avtorji izvedli z rentgensko energijsko difrakcijsko spektroskopijo (EDX) in infrardečo spektroskopijo s Fourierjevo transformacijo (FTIR). FTIR spektrum je potrdil prisotnost bio filma in s pomočjo vrstične selektronske spektroskopije (SEM) so le tega skupaj s korozijskimi usedlinami morfološko opredelili oziroma ovrednotili. Avtorji na osnovi analiz ugotavljajo, da je začetek nastajanja korozijskih oblog posledica zagonov in ustavitev obratovanja termoelektrarne. Rezultati analiz so pokazli tudi, da je prišlo do jamičaste korozije zaradi mikroorganizmov, ki se nahajajo v biofilmu in so odporni na baker. Glavna prednost in spoznanje pridobljeno s temi analizami je definiranje postopkovnega sistema s katerim naj bi se čimbolj izognili ustavitvam in ponovnim zagonom obratovanja termoelektrarne.

Ključne besede: jamičasta korozija, termoelektrarna, kondenzator

1 INTRODUCTION

Tubes from the shell and tube condenser that use cooling seawater in a coastal thermal power plant that encountered frequent leakages, were investigated in order to determine the cause of corrosion. The thermal power plant TE Plomin 2 Block B has a nominal load of 217 MW, a high-pressure steam boiler of 670 t/h (147.4 bar/535 °C) using coal as fuel. The efficiency of the boiler is 92.9 % with a thermal power of 544 MW. The condenser with 12,000 tubes of the steam turbine is cooled by sea water in one pass, and the intake of cooling water is located at the Plomin Bay at a depth of 24 m. The amount of steam is 116.36 kg/s and the pressure is 0.046 bar with a dryness of 91 % while the cooling water flow is 86,677 kg/s; the intake temperature is 20 °C and the outlet temperature is 27.5 °C. A pH value of 8.83 and oxygen concentration of 79 mg/L in February proved that the cooling water taken from deep water intake is saturated with oxygen, having the pH value in the normal range. A test of the sea water showed that $NH_3 < 0.1$ mg/L, Cu < 2 mg/L, Fe < 2 mg/L, and silicon dioxide average is 0.0021 mg/L. The average salinity of the Adriatic Sea is around 38.3 ‰ while the average salinity of the ocean is 35 ‰. The tubes were made of CuZn20Al2As alloy and were declared to conform to the EN 12451 and VGB-R 106e standard guidelines.[1] The length of a tube is 11,920 mm. The operating environment conditions within the tube condenser can cause

*Corresponding author's e-mail:
mkrsulja@unipu.hr

premature failure of tubing and piping. In some cases these include an inadequate ferrous sulphate addition and a high level of chlorination.[2] In other cases, the failure of condenser tubes is microbially influenced by a biofilm formation of copper-tolerant microorganisms.[3,4] A failure of the condenser brass tube in thermal power units is caused by a failure of the condenser cooling tube, which is an occurring problem.[2–5] The tube interior includes the water side of the condenser, and the velocity of seawater inlet at an unstable or high degree of turbulence can also lead to corrosion of copper alloys. The corrosion rate was evaluated and the copper loss was 60 mg/L at a cooling water flow of 8677 kg/s. The flow velocity varies from 5.5 ms^{-1} to 8.5 ms^{-1} and the calculated flow rate equals 1.89 m^3s^{-1}, which is lower than the maximum allowable flow rate of 2 m^3s^{-1}, specified by the tube manufacturer. The system operates in the once-through mode. The seawater inlet temperature varies from 12 °C to 21 °C and the outlet temperature varies from 18 °C to 28 °C. In order to execute the overhaul, the power plant is shut down for an average of 30 days per year when the condenser tubes are emptied of the seawater. The cause and type of corrosion are investigated to avoid the need for a tube replacement and to lessen the intensity of failure of the power plant that cause high financial losses.

2 EXPERIMENTAL PART

For the investigation of a tube specimen made from CuZn20Al2As, several methods and types of equipment were used. A GDS500A LECO optical emission spectrometer was used for determining the chemical compositions of metals and alloys, together with the incandescent discharge method and 99.999 % argon.

A microhardness test was carried out according to HRN EN ISO 6507-1: 2018.[6] A metallographic analysis, a light microscope analysis, was performed with an Olympus BX51 metallographic microscope. Scanning electron microscopy (SEM) and energy dispersive X-ray spectroscopy (EDS) that allow a targeted analysis of sample surfaces were conducted with a QUANTA FEG 250 SEM FEI scanning electron microscope with field emission and OXFORD PENTA FET EDS detector.

An EDS microanalysis of the chemical compositions of solid materials was carried out using FE SEM (SEM), a HighVacumm secondary electron detector with 20 kV and a spot size of 5 μm. A FT-IR spectroscopy analysis of the chemical composition was carried out with IR spectroscopy, and KBr tablets were made using a Tensor 27 FT-IR spectroscope. The spectra were the result of the mean value of 64 recorded spectra for a single sample, and the recording resolution was 4 cm^{-1}. The values of the obtained bands are marked on the spectrum.

3 RESULTS

3.1. Visual and optical microscopy analysis

Two tube segments were examined visually and microscopically, one with a rupture and one without any rupture. Photographs of both tube segments are shown in **Figures 1a** and **1b**, the condenser is shown in **Figure 1c** and the positioning of tubes in the condenser is shown in **Figure 1d**. In general, the entire steam side of the investigated tube segments was covered with a uniform, brown, thin and well-adhering layer of copper patina except for the areas with a partially faded oxide band, showing that the tubes were in direct contact with the baffle plate. Also, the ruptured-tube shape indicated a tube bending over the baffle plate. No other corrosion or erosion defects were found at the steam side of the tubes.

The rupture was situated within the faded oxide band; the thickness of the tube was around 1 mm. The steam

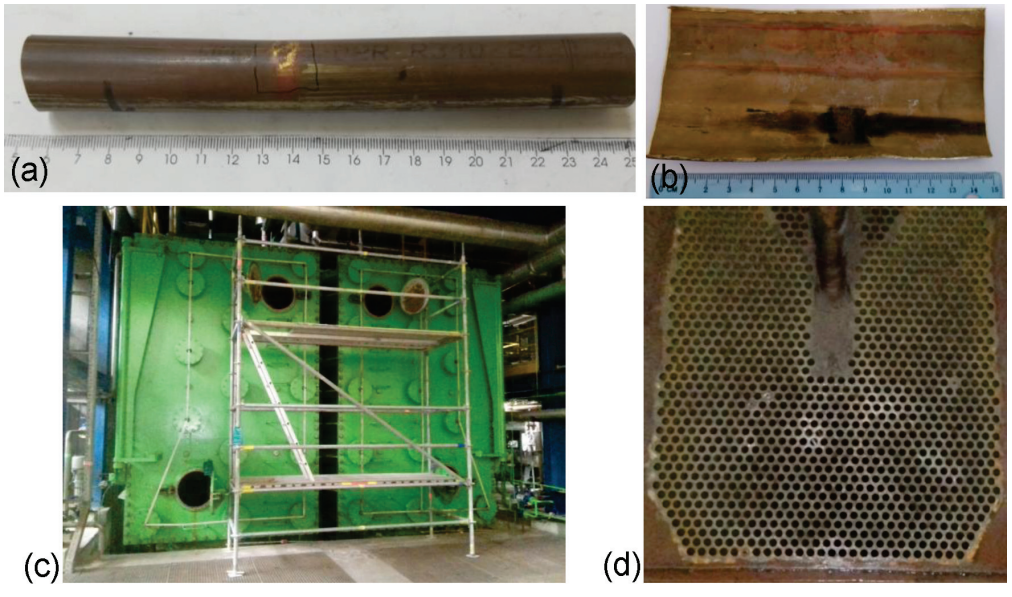

Figure 1: Photographs of: a) the ruptured tube segment, b) the interior of the non-ruptured tube segment, c) condenser, d) tubes in the condenser

Figure 2: Microscopic images of the investigated rupture at: a) the steam side of the tube and b) the water side, magnification of 50×

Table 1: Mean values of the measured mass fractions (w/%) of individual elements in the sample expressed as percentage (%)

	Zn	Al	Fe	Ni	Si	Bi	As	S	Cu
Average	21.41	2.201	0.0199	0.0492	0.0398	0.0226	0.0865	0.0026	76.17

side of the tube in the immediate area of rupture is shown enlarged in **Figure 2a**. At the water side of the tube, the same rupture was observed within the localized pit of an irregular shape (**Figure 2b**), while the rest of the surface in the immediate vicinity was covered by a cracked light-brown layer of corrosion products, through which red and black sublayers were visible. The bottom of the pit was black.

At the water side of the tubes, adjacent to the supposed contact with the baffle plates, the areas of red and black discolouration were visible below the golden-brown cracked layer (**Figure 1b**). The circumference position of these thick corrosion-product deposits varied depending on the baffle-plate contact spot. On the supposedly bottom part of the tube, from approximately 5:00–7:00 hours, a reddish-brown layer extended along the tube. Shallow pitting damage was evident within that area in the form of individual pits or clusters of smaller pits.

The rest of the water side was covered with a uniform, thin, golden-brown layer. No significant corrosion damage was observed in that area and it could be concluded that the layer protected the metal well. A similar layer was observed[7] on copper alloys under the influence of flowing (1.5 ms^{-1}) aerated seawater at a temperature > 40 °C. At temperatures between 20 °C and 30 °C, this layer is usually darker, brown and partially adherent, and a dark-brown, well adhered layer is formed at temperatures below 10 °C.

3.2. Chemical analysis

Table 1 shows the chemical composition of the CuZn20Al2As alloy. Except for arsenic (As), all the elements of the alloy are within the permissible limits given by EN 12451. The sum of bismuth (Bi), silicon (Si) and sulphur (S) contents does not exceed 0.3 %, which satisfies the requirement that the metals, other than those with prescribed percentages, should not be present in an amount greater than 0.3 %. The percentage of arsenic (0.0865 %) is slightly higher than its limit (0.06 %). Arsenic (As) is added to brass to reduce corrosion and dezincification, so its slightly higher concentration probably does not adversely affect the corrosion properties of the test alloy.

3.3. Metallographic, microhardness and Fourier transform infrared analysis

A metallographic sample was cold cut, ground and polished in several steps to achieve a flat surface, cleaned and etched with the ASTM No. 30 reagent for 30 seconds and then dried before measuring. A metallographic analysis of the tube material has shown that the investigated brass consisted solely of the α phase (**Figure 3 a**), which is a solid solution of zinc and other alloying elements in copper. No aggregates or precipitates were observed. At a magnification of 200× annealing twins were observed, indicating that the metal was heat treated[8]. The grain size was in a range of 10–50 µm as prescribed by the HRN EN ISO 12451 standard for the CuZn20Al2As alloy.[9] This type of brass microstructure was proven to be the most resistant to corrosion.[10]

The microhardness of the tube material, CuZn20Al2As brass, was determined according to EN ISO 6507-1 and equalled 107.4 ± 0.5 HV. The specified value was <110 HV, therefore in accordance with the requirement of EN 12451. The sample of corrosion products for the FT-IR analysis was taken from the steam side

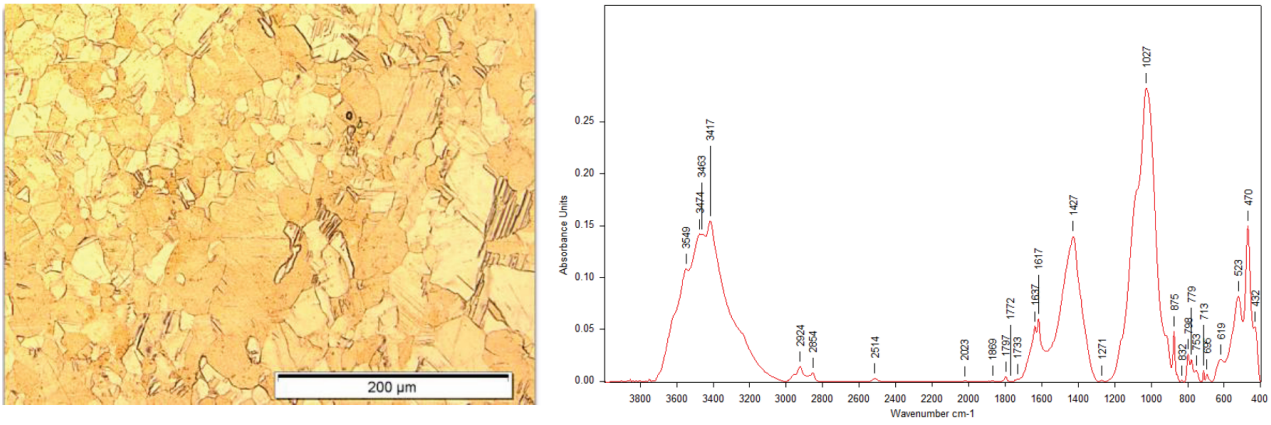

Figure 3: a) Microscopic image of the metallographic sample, b) the FT-IR spectrum of corrosion products

of the ruptured-tube segment, from around the rupture site (**Figure 3 b**).

The spectrum largely corresponds to the illite mineral (clay material) with a composition of $(K_2H_3O)(Al_2Mg_2Fe)_2(Si_2Al)_4O_{10}$ $[(OH)_2,(H_2O)]$, which probably originates from the seawater. The bands at (798, 875, 1427, 1797) cm^{-1} and the bands in the range of 2800–3000 cm^{-1} coincide with the spectrum of calcium carbonate. The bands at (713, 875, 1027, 1271, 1427, 1617 and 1637) cm^{-1} correspond to the spectrum of the standard biofilm containing polysaccharides and proteins[11].

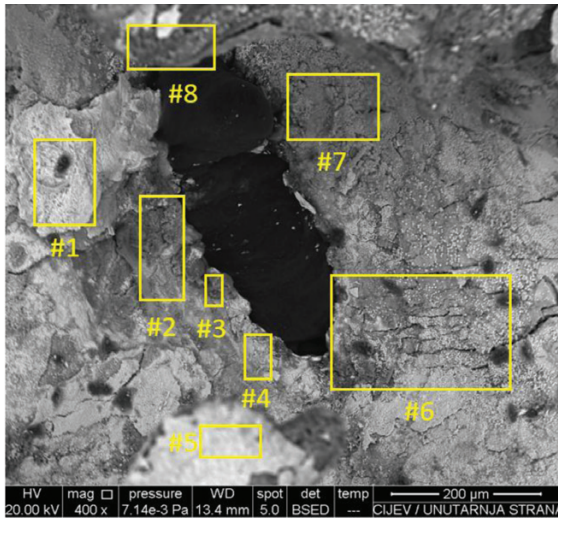

Chemical composition, *w*/%								
	#1	#2	#3	#4	#5	#6	#7	#8
Cu	87.95	34.39	52.98	77.58	41.30	73.45	44.66	27.81
Zn	2.46	12.87		12.73	6.68	6.40	14.14	6.86
C	4.97	26.81		6.48	21.50	14.64		28.51
O	3.18	25.92	36.77	3.21	16.15	1.47	32.56	21.78
Al	0.24		3.81		0.73	1.13	3.33	2.36
Si	0.21		3.13		1.02	1.49	2.22	4.06
S	0.35		3.31		9.09	1.41	3.08	3.85
Fe	0.64				2.80			2.97
Ca					0.40			0.55
Mg								0.67
K								0.59
Cl					0.32			

Figure 4: Composition obtained with the EDS microanalysis of the tube water side

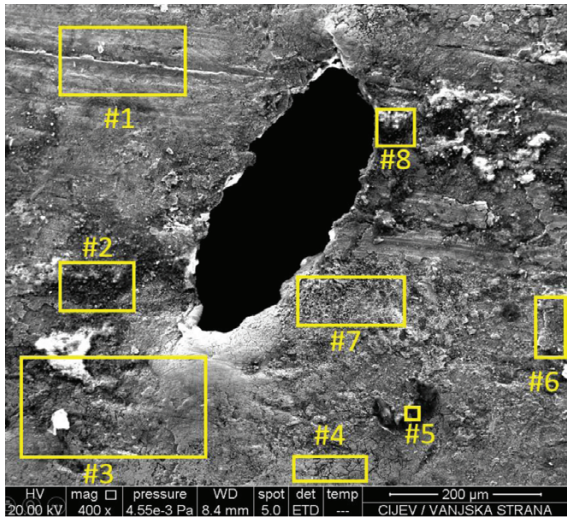

Chemical composition, *w*/%								
	#1	#2	#3	#4	#5	#6	#7	#8
Cu	55.44	32.97	56.93	60.13	33.79	54.98	62.00	35.02
Zn	10.74	4.11	11.96	15.48	7.09	2.66		3.73
C	21.25	33.48	21.57	16.82	51.10	19.50	26.47	36.00
O	8.55	19.89	6.84	5.68	7.21	15.69	9.97	14.70
Al	0.87	1.87	0.67	1.52	0.29			1.57
Si	0.21	3.06	0.56		0.12		0.26	2.95
S	0.16	0.25			0.21		0.19	0.24
Fe	1.25	0.74	0.38			5.64	0.30	1.28
Ca	0.24	1.83					0.16	2.95
Mg	0.29	1.15				0.52		0.56
K		0.29				0.28		0.38
Cl		0.36	0.86	0.36	0.18	0.43	0.66	0.51

Figure 5: Composition obtained with the EDS microanalysis of the tube steam side

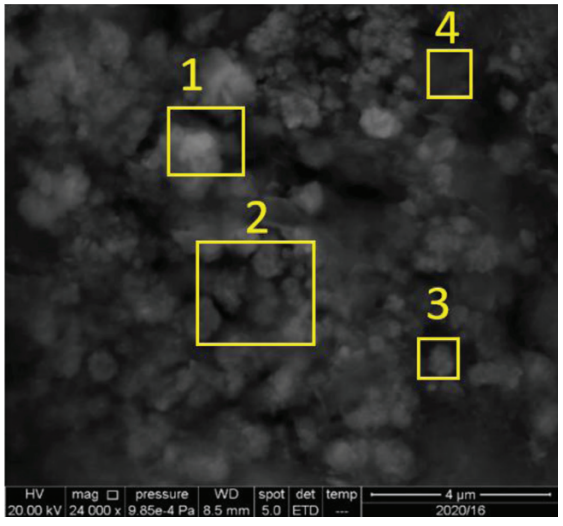

Chemical composition, as measured, %				
	#1	#2	#3	#4
Cu	6.39	39.66	27.25	3.48
Zn	24.57	14.08	13.64	3.01
C	23.27	22.34	28.30	25.09
O	27.81	10.96	18.03	39.64
Al	4.07	2.05	2.46	4.97
Si	3.98	1.46	1.75	10.15
S	0.61	6.99	4.01	0.57
Fe	4.87	0.89	0.99	3.11
Ca	0.49		1.54	5.12
Mg	3.94	1.14	1.26	1.47
K			0.31	1.58
Cl		0.44	0.46	0.63

Figure 6: Black corrosion-product layer on the water side

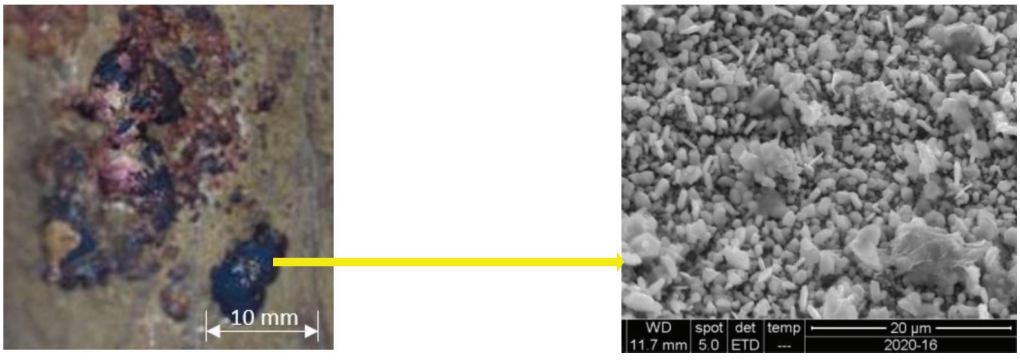

Figure 7: Sample cleaned a) in 10 % citric acid, b) in 2 M HCl

3.4 SEM/EDS analysis

SEM micrographs and EDS chemical composition of the immediate vicinity of the rupture site for the water side are shown in **Figure 4**, and for the steam side, they are shown in **Figure 5**. Eight measuring points were added to better observe the difference in the chemical composition of different areas of the surface and obtain the mean values. The most common elements found with the EDS analysis were copper, zinc, carbon and oxygen (Cu, Zn, C and O), indicating the composition of the substrate, and probably the formation of oxides and carbonates of copper. There is also Al, which probably originates from the substrate and is known to be embedded into the protective brass patina[7] in the form of Al_2O_3. Silicon (Si) and sulphur (S) are also components of the alloy, but both of them, in particular S, occurred in the EDS analysis in excess compared to their alloy content (**Table 1**). Therefore, these elements are also likely to originate from the environment, along with calcium (Ca), magnesium (Mg), potassium (K) and chlorine (Cl). Iron may originate from the previous treatments with ferrous sulphate that forms a protective layer of lepidocrocite (γ – FeOOH) on the copper surface.

The SEM micrograph of the black corrosion-product layer on the water side, shown in **Figure 6**, features blurred areas that probably correspond to the biofilm. The EDS elemental composition recorded at four sites over a larger area than that shown by the micrograph has again demonstrated high sulphur concentrations.

The ruptured sample was further subjected to cleaning in 10 % citric acid and then in 2 M HCl. The residual black deposits at the bottom of the previously investigated pit (**Figure 7 a**) were further analysed with SEM/EDS (**Figure 7 b**). The deposits consisted of polygonal crystals and their composition is presented in **Table 2.**

Table 2: Mean values of the measured mass fractions (*w*/%) of individual elements in the sample expressed as percentage (%)

Cu	Zn	C	O	Al	Si	S
63.52	8.46	8.35	5.44	1.08	0.86	12.29

The absence of all other elements, except the elements present in the substrate and the extremely high percentage of sulphur, however, indicates the likely presence of sulphide at the bottom of the pit.[12]

4 DISCUSSION

The corrosion and rupture of the condenser tubes considered in this study were of a strictly localized character and initiated at the water side. In this study, no

traces of erosion or corrosion-erosion damage, flow damage due to turbulence or jet-impact damage were found.

However, we did find cavities or holes assumed to be pit holes that contained corrosion products. Therefore, it was assumed that the corrosion damage was pitting corrosion because, as observed through the pit, it had a somewhat elliptical shape. Pitting can be initiated by localised chemical or mechanical damage made to the protective oxide film by accident. It can also be caused by localised damage made to a coating or the presence of non-metallic inclusions in the metal structure. Pitting is a result of an abnormal anodic area surrounded by a normal surface that acts as a cathode that influences the localised loss in the thickness. The thickness loss can be narrow and deep, shallow and wide, elliptical, vertical grain attack, subsurface, undercutting or horizontal grain attack.

The shallow pitting at the bottom of the tubes was assumed to be initiated under the water where sediments were retained after the draining of cooling seawater due to periodic emptying of the system. However, the thickest corrosion products and the most intensive corrosion attack were concentrated at the water side of the tubes, adjacent to the contact between the tubes and the baffle plates. This observation indicated that pitting corrosion was preferentially influenced by the local conditions at that site.

The observed form of corrosion could be characterized as the corrosion beneath the deposits. The mechanism of this corrosion is based on the emergence of the so-called differential aeration cell.[12] Below the deposit, which can be of inorganic (mud, sand) or organic (biofilm) origin, oxygen depletion occurs due to the physical sheltering of that space and oxygen consumption in the corrosion reaction or by aerobic bacteria in the biofilm. At the oxygen-depleted site, the metal begins to dissolve predominantly (anode surface), and at the sites where oxygen is more readily available, a cathodic corrosion reaction of oxygen reduction (cathode surface) predominantly occurs. Additionally, at the pit bottom, anaerobic bacteria may become active. The phenomenon of underdeposit corrosion can be especially pronounced during a shutdown when inorganic and organic deposits are likely to form. After emptying the system, the cooling water may not be completely drained and may reside at the bottom of the tubes supporting high-humidity conditions. Under the same conditions, water droplets or areas of the moistened layer of deposits may also exist at the top of the tubes for a long time. Such moist, stagnant areas would be suitable for the development of microorganisms.

In the presence of anaerobic sulphate-reducing bacteria, corrosion can be further accelerated[12]. These anaerobic bacteria are active in the niches where anaerobic conditions prevail. As a product of metabolism of these bacteria, sulphide ions are formed which react with copper and black copper sulphide is produced. Sulphides are highly corrosive to copper and copper alloys.[7] Sulphides can also be present in seawater as a product of industrial waste[13] or metabolism of marine cultures.[14] With the presence of sulphides in very small amounts of a few tens of μg/L, in solutions containing chlorides, the corrosion products formed on pure copper and copper alloys are not compact and do not provide good protection.[15] It should be noted that the cooling circuits of seawater-cooled power plants act as incubators for microorganisms because they represent an aquatic environment of an appropriate temperature (usually between 30 °C and 60 °C) and a pH of 6 to 9, supporting microorganism growth and providing a continuous source of organic and inorganic nutrients.[6]

The location of thick corrosion products at the water side just below the buffer plate may point to the specific influence of the temperature on the formation of deposits. This phenomenon is referred to in the literature as hot-spot corrosion.[16] This corrosion occurs at a site of the overheating of the wall due to the high local temperature on the steam side, i.e., due to the increased heat transfer in the area of contact between the tube wall and the supporting wall. Overheating and even distortion of a tube, which was observed on the ruptured tube, may occur when re-starting the system after a shutdown period, if the condenser is steam-filled and there is not enough cooling water in the system. Therefore, when starting the system after a shutdown, special care must be taken to avoid the overheating of the tube wall. One-time sudden heating can trigger the cracking of the protective layer, leading to the development of corrosion during the system operation. Support flanges of the condenser were made from S235JR (1.0038) EN 10025-2: 2004, old designation: 1.0037 material RSt 37-2, DIN 17120. The degree of expansion of the flanges and piping material on the condenser was not investigated.

5 CONCLUSIONS

The main cause for the shutdown of the above thermal power plant was leakage of the cooling-system condenser tubes due to the corrosion caused by the pitting mechanism. Pitting was caused by biofilm microorganisms, chemically damaging the CuZn20Al2As tubes.

Any inhomogeneity of the condenser tube walls could be a potential site for the initiation of corrosion. The tube water-side areas adjacent to the contact with the buffer plates as well as the bottom area of the tubes were found to be the predominant sites of corrosion and niches for bacterial growth. Deposits in both critical areas were assumed to be linked to the shutdown periods of the condenser when it was emptied of the seawater, as well as to the system startup after the shutdown period. Underdeposit corrosion that occurs trough differential aeration cells aggravated by the action of bacteria was diagnosed.

6 REFERENCES

[1] VGB-R 106e Guideline, Tubes for Condensers and Other Heat Exchangers for the Operation of Steam Turbine Plants – Copper Alloys, VGB PowerTech e.V, 2012, https://www.vgb.org/shop/r106e.html?__store=en&___from_store=default, 15.03.2022

[2] T. S. Rao, S. Bera, Protective layer dissolution by chlorine and corrosion of aluminum brass condenser tubes of a nuclear power plant, Engineering Failure Analysis, 123 (**2021**), doi:10.1016/j.engfailanal.2021.105307

[3] T. S. Rao, K. V. Nair, Microbiologically influenced stress corrosion cracking failure of admiralty brass condenser tubes in a nuclear power plant cooled by freshwater, Corrosion Science, 40 (**1998**) 11, 1821–1836, doi:10.1016/S0010-938X(98)00079-1

[4] M. L. Carvalhoa, J. Domabc, M. Sztylerb, I. Beech, P. Cristiania, The study of marine corrosion of copper alloys in chlorinated condenser cooling circuits: The role of microbiological components, Bioelectrochemistry, 97 (**2014**), 2–6, doi:10.1016/j.bioelechem.2013.12.005

[5] N. X. Xiao, F. W. Wei, M. G. Jun, B. S. Qi, S. Zang, Failure analysis of the condenser brass tube in 150 MW thermal power units, Engineering Failure Analysis, 33 (**2013**), 75–82, doi:10.1016/j.engfailanal.2013.04.026

[6] Microhardness test – HRN EN ISO 6507-1: 2018, http://repozitorij.hzn.hr/norm/HRN+EN+ISO+6507-1%3A2018, 15.3.2022

[7] M. L. Carvalho, Corrosion of copper alloys in natural seawater: effects of hydrodynamics and pH, PhD Thesis, Université Pierre et Marie Curie, Paris VI, 2014, https://hal.science/tel-01089313/document

[8] T. Liptakovaa, J. Broncekb, M. Loviseka, J. Lagoa, Tribological and corrosion properties of Al-brass, Materials Today, 4 (**2017**), 5867–5871, doi:10.1515/kom-2017-0010

[9] HRN EN ISO 12451 for CuZn20Al2As alloy, https://repozitorij.hzn.hr/norm/HRN+EN+12451%3A2013, 15.3.2022

[10] E. Stålnacke, E. Claesson, C. Obitz, M. Lilja, J. Odqvist, J. Hagström, O. Rod, Corrosion–microstructure interrelations in new low-lead and lead-free brass alloys, Materials Science and Technology, 36 (**2020**) 8, 917–924, doi:10.1080/02670836.2018.1489619

[11] Z. Zhang, R. Cai, W. Zhang, Y. Fu, N. Jiao, A Novel Exopolysaccharide with Metal Adsorption Capacity Produced by a Marine Bacterium Alteromonas sp. JL2810, Mar. Drugs, 15 (**2017**) 6, 175, doi:10.3390/md15060175

[12] W. Moore, Power station condensers their design and failure modes, Materials at High Temperatures, 34 (**2017**) 5–6, 407–414, doi:10.1080/09603409.2017.1370191

[13] Q. Mahmood, P. Zheng, J. Cai, H. Yousaf, H. M. Jaffar, W. Dong-lei, H. Bao-Ian, Sources of sulfide in waste streams and current biotechnologies for its removal. J. Zhejiang Univ. – Sci. A, (**2007**) 8, 1126–1140, doi:10.1631/jzus.2007.A1126

[14] X. Hu, J. Liu, H. Liu, G. Zhuang, L. Xun, Sulfur metabolism by marine heterotrophic bacteria involved in sulfur cycling in the ocean, Sci. China Earth Sci., 61 (**2018**), 1369–1378 doi:10.1007/s11430-017-9234-x

[15] C. D. S. Tuck, C. A. Powell, J. Nuttall, Corrosion of Copper and its Alloys, in: Reference Module in Materials Science and Materials Engineering, 2016, doi:10.1016/b978-0-12-803581-8.01634-9

[16] W. Faes, S. Lecompte, Z. Y. Ahmed, J. Van Bael, R. Salenbien, K. Verbeken, M. De Paepe, Corrosion and corrosion prevention in heat exchangers, Corrosion Reviews, 37 (**2018**) 2, 131–155, eISSN 2191-0316